11-2012

Quantifying nonisothermal subsurface soil water evaporation

Pukhraj Deol
North Carolina State University at Raleigh

Josh Heitman
North Carolina State University at Raleigh

Aziz Amoozegar
North Carolina State University at Raleigh

Tusheng Ren
China Agricultural University

Robert Horton
Iowa State University, rhorton@iastate.edu

Quantifying nonisothermal subsurface soil water evaporation

Abstract
Accurate quantification of energy and mass transfer during soil water evaporation is critical for improving understanding of the hydrologic cycle and for many environmental, agricultural, and engineering applications. Drying of soil under radiation boundary conditions results in formation of a dry surface layer (DSL), which is accompanied by a shift in the position of the latent heat sink from the surface to the subsurface. Detailed investigation of evaporative dynamics within this active near-surface zone has mostly been limited to modeling, with few measurements available to test models. Soil column studies were conducted to quantify nonisothermal subsurface evaporation profiles using a sensible heat balance (SHB) approach. Eleven-needle heat pulse probes were used to measure soil temperature and thermal property distributions at the millimeter scale in the near-surface soil. Depth-integrated SHB evaporation rates were compared with mass balance evaporation estimates under controlled laboratory conditions. The results show that the SHB method effectively measured total subsurface evaporation rates with only 0.01–0.03 mm h−1difference from mass balance estimates. The SHB approach also quantified millimeter-scale nonisothermal subsurface evaporation profiles over a drying event, which has not been previously possible. Thickness of the DSL was also examined using measured soil thermal conductivity distributions near the drying surface. Estimates of the DSL thickness were consistent with observed evaporation profile distributions from SHB. Estimated thickness of the DSL was further used to compute diffusive vapor flux. The diffusive vapor flux also closely matched both mass balance evaporation rates and subsurface evaporation rates estimated from SHB.

Keywords
evaporation, heat transfer, soil water

Disciplines
Agriculture | Hydrology | Soil Science

Comments
This article is published as Deol, Pukhraj, Josh Heitman, Aziz Amoozegar, Tusheng Ren, and Robert Horton. "Quantifying nonisothermal subsurface soil water evaporation." Water Resources Research 48, no. 11 (2012). doi: 10.1029/2012WR012516. Posted with permission.

Quantifying nonisothermal subsurface soil water evaporation

Pukhraj Deol,[1] Josh Heitman,[1] Aziz Amoozegar,[1] Tusheng Ren,[2] and Robert Horton[3]

Received 11 June 2012; revised 17 September 2012; accepted 26 September 2012; published 2 November 2012.

[1] Accurate quantification of energy and mass transfer during soil water evaporation is critical for improving understanding of the hydrologic cycle and for many environmental, agricultural, and engineering applications. Drying of soil under radiation boundary conditions results in formation of a dry surface layer (DSL), which is accompanied by a shift in the position of the latent heat sink from the surface to the subsurface. Detailed investigation of evaporative dynamics within this active near-surface zone has mostly been limited to modeling, with few measurements available to test models. Soil column studies were conducted to quantify nonisothermal subsurface evaporation profiles using a sensible heat balance (SHB) approach. Eleven-needle heat pulse probes were used to measure soil temperature and thermal property distributions at the millimeter scale in the near-surface soil. Depth-integrated SHB evaporation rates were compared with mass balance evaporation estimates under controlled laboratory conditions. The results show that the SHB method effectively measured total subsurface evaporation rates with only 0.01–0.03 mm h^{-1} difference from mass balance estimates. The SHB approach also quantified millimeter-scale nonisothermal subsurface evaporation profiles over a drying event, which has not been previously possible. Thickness of the DSL was also examined using measured soil thermal conductivity distributions near the drying surface. Estimates of the DSL thickness were consistent with observed evaporation profile distributions from SHB. Estimated thickness of the DSL was further used to compute diffusive vapor flux. The diffusive vapor flux also closely matched both mass balance evaporation rates and subsurface evaporation rates estimated from SHB.

Citation: Deol, P., J. Heitman, A. Amoozegar, T. Ren, and R. Horton (2012), Quantifying nonisothermal subsurface soil water evaporation, *Water Resour. Res.*, *48*, W11503, doi:10.1029/2012WR012516.

1. Introduction

[2] Accurate quantification of energy and mass transfer during soil water evaporation is critical for improving our understanding of large scale hydrologic and climatic patterns as well as for many environmental, agricultural, and engineering applications. Soil water evaporation has frequently been considered a three stage process [*Lemon*, 1956; *Feddes*, 1971; *Idso et al.*, 1974] starting with a relatively high and constant evaporation rate (stage 1) followed by a falling rate (stage 2), and eventually shifting to a very low and relatively constant rate (stage 3). During stage 1, water is available at the soil surface and evaporation is limited by atmospheric evaporative demand [*Lemon*, 1956]. At this stage, a large portion of the surface net radiation is readily dissipated as latent heat of vaporization. With progressive drying, the surface soil comes in equilibrium with the overlying air and it becomes approximately air-dry [*Hillel*, 1980]. This results in formation of a dry surface layer (DSL), also referred to as "soil mulch" [*Kimball*, 1973], which acts as a barrier to liquid water flow from moist subsurface soil to the dry soil surface [*Jalota and Parihar*, 1998]. This process also has a significant effect on heat and mass transfer within the soil [*Liu et al.*, 2005]. *Hillel* [1971] and *Campbell* [1985] reported that vaporization of water occurs at the bottom boundary of the DSL. This was confirmed by laboratory [*Yamanaka et al.*, 1997] and numerical experiments [*Yamanaka et al.*, 1998], which concluded that in addition to the vaporization occurring at the bottom boundary of the DSL, transient vaporization or condensation also occurs within the DSL when there are notable changes in soil temperature [*Yamanaka and Yonetani*, 1999]. Recently, *Novak* [2010] studied dynamics of the near-surface evaporation zone numerically in a bare, drying silt-loam soil under clear sky conditions and observed a strong diurnal pattern superimposed on interdiurnal changes associated with progressive drying. The *Novak* [2010] simulation indicated that the transition between surface and subsurface evaporation occurred daily early in the drying period, and it affected the surface energy balance and near-surface temperature and water content profiles.

[3] Radiant energy fluxes at a dry soil surface in a field environment result in steep temperature gradients, making

[1]Department of Soil Science, North Carolina State University, Raleigh, North Carolina, USA.
[2]China Agricultural University, Beijing, China.
[3]Iowa State University, Ames, Iowa, USA.

Corresponding author: J. Heitman, Department of Soil Science, North Carolina State University, PO Box 7619, Raleigh, NC 27695-7619, USA. (josh_heitman@ncsu.edu)

0043-1397/12/2012WR012516

the surface soil heat flux a large fraction of the surface energy budget [*de Vries and Philip*, 1986; *Mayocchi and Bristow*, 1995; *Heitman et al.*, 2010]. Partitioning of this surface heat flux between latent and sensible heat within soil depends on tightly linked thermal and hydraulic processes. Soil thermal properties control the energy available for subsurface evaporation by influencing conduction heat flow and sensible heating, while soil hydraulic properties control the rate of liquid water supply from the moist subsurface to the evaporation zone, as well as the rate of vapor loss from the soil surface. The depth of soil drying or location of the evaporation front depends on the balance between transfer rates of heat, liquid, and vapor [*Bitelli et al.*, 2008]. Previous studies by *Idso et al.* [1974] recognized a connection between changes in surface albedo (indicating surface drying) and the onset of falling-rate evaporation, suggesting a loss of liquid water connectivity to the surface at the beginning of stage-2 evaporation. *Idso et al.* [1975] further connected falling rate evaporation to the soil energy budget, making use of increasing soil surface temperatures to mark the transition to falling-rate evaporation.

[4] Several recent studies have attempted to better elucidate soil hydraulic controls on evaporation through experiment, focusing on differences between early and late stage evaporation. By measuring evaporation from an initially saturated porous media under isothermal conditions, *Shokri and Or* [2011] reported "jumps" in the evaporation front from the surface to the subsurface at the end of stage 1. They reported that the jump length is affected primarily by porous media properties. *Shokri and Salvucci* [2011] related the low rate of evaporation during late stage evaporation to the water table depth at which the liquid water connection to the surface is lost for several sand materials under isothermal conditions. *Shokri and Or* [2011] emphasized the need for further investigation to accurately characterize the abruptness and dynamics of the important transition from high rate to low rate stage evaporation (i.e., stage 1 to stage 3). Most soil water evaporation in arid regions occurs during stage 2 [*Brutsaert and Chen*, 1995; *Snyder et al.*, 2000; *Ventura et al.*, 2001] and under nonisothermal, transient conditions, which further emphasizes the need to thoroughly investigate this important transition in evaporation regimes, as well as related implications for the surface energy budget.

[5] To date, few attempts have been mato quantify subsurface evaporation profiles, especially under nonisothermal, transient conditions. This requires detailed fine-scale investigation of the highly dynamic near-surface zone. Measurements necessary to capture the dynamics in the near-surface zone, however, are very challenging which is presumably a main reason for related knowledge gaps in the soil water evaporation literature on transitions between early and late stage evaporation. A sensible heat balance (SHB) approach based on fine-scale temperature and thermal property measurements in the near-surface zone has been proposed to estimate subsurface, nonisothermal evaporation under transient conditions [*Heitman et al.*, 2008b, 2008c]. The SHB approach estimates latent heat flux for a soil layer as the residual to a balance between the divergence in sensible heat flux across the layer and the change in sensible heat storage for the soil layer. Field experiments [*Heitman et al.*, 2008b, 2008c; *Xiao et al.*, 2011] and model evaluations [*Sakai et al.*, 2011] indicate that the SHB approach is accurate for measuring in situ, subsurface soil-controlled evaporation. The main limitation of the SHB approach in these studies was the inability of instrumentation to quantify evaporation during the initial shift between surface and subsurface evaporation, when evaporation occurs at depths shallower than approximately 3 mm [*Sakai et al.*, 2011]. Specifically, depth resolution was constrained by the 6 mm needle spacing of the three-needle probe design used in the original SHB studies to measure near-surface temperature gradients. Recent adaptations to the probe design, with closer needle spacing near the surface, have narrowed this "undetectable" zone to as shallow as 0.5 mm soil depth (i.e., the midpoint between the shallowest temperature sensing needles at 0 and 1 mm depths) [*Zhang et al.*, 2012]. Full realization of the potential of the SHB approach, using improved instrumentation, requires further testing and evaluation.

[6] Considering the knowledge gaps for evaporation, especially related to the transition between atmospherically controlled and late stage evaporation under nonisothermal conditions, and the potential utility of the measurement-based SHB approach to study the highly dynamic near-surface layer, we conducted experiments with three primary objectives: (1) evaluate SHB-estimated evaporation under controlled laboratory nonisothermal conditions by comparing it with mass balance evaporation estimates; (2) quantify subsurface, nonisothermal evaporation profiles during falling rate evaporation; and (3) examine the development of the DSL during falling rate evaporation.

2. Materials and Methods

2.1. General Experimental Setup and Soil Properties

[7] Studies were conducted under controlled laboratory conditions to allow data collection during a continuous drying event and to have an accurate mass evaporation estimate to validate the SHB-estimated evaporation. Nonisothermal conditions were chosen to simulate drying under radiation boundary conditions common in the field. A steady state evaporation study was conducted first to test SHB approach under simple conditions. A transient evaporation study was also performed to quantify subsurface evaporation profiles over a drying event. A 34 cm long open top column, constructed of 6 in. (15.25 cm inside diameter) polyvinyl chloride (PVC), was packed with sand material, similar to that used by *Arya et al.* [2008, 2010], at a uniform bulk density of 1.65 g cm^{-3}. The bottom of the column was connected to a Marriott bottle to wet the soil from the bottom and also to control the saturated zone within the column (Figure 1a). The soil column and Marriott bottle were placed on separate weighing scales for measuring the mass losses of water. Mass losses of water from the soil column and Marriott bottle were manually recorded at 0.1 g resolution using separate digital scales. A ceramic heat emitter was installed at 20 cm distance above the column to uniformly heat the soil surface.

[8] The particle size distribution of the sand material is given in Table 1 (adapted from *Arya et al.* [2008]); saturated hydraulic conductivity is 2.8 m h^{-1}. Wet end water retention at zero (saturation) to 100 cm tension (equivalent to −100 cm soil water pressure head) was determined destructively following *Howard et al.* [2010] (Figure 2;

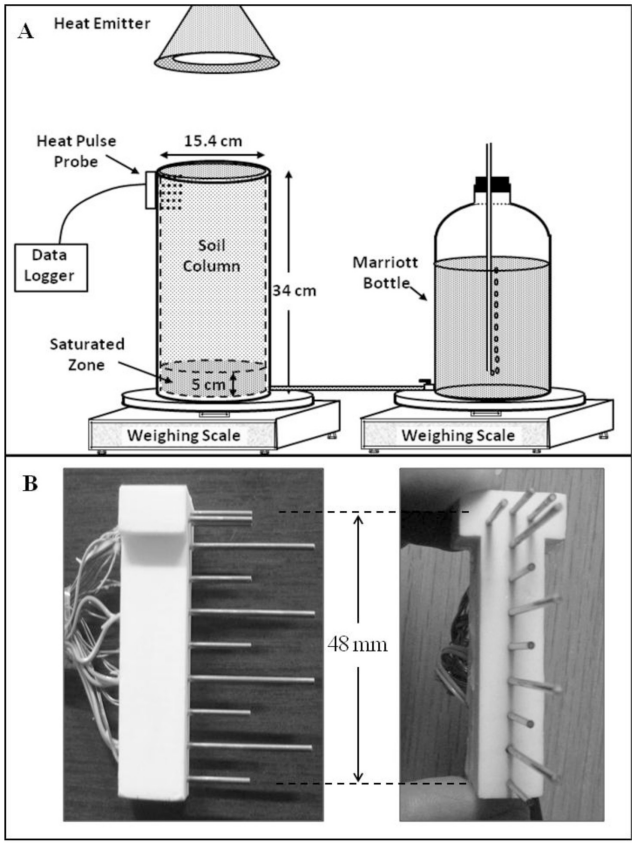

Figure 1. (a) Setup for soil column experiments. The Marriott bottle was disconnected for transient experiments. (b) Multineedle heat-pulse probe used in the experiments. All 11 needles contain thermocouples. The four long needles also contain a resistance heater. Spacing between adjacent needles is 6 mm for needles positioned along the vertical midline of the probe. The upper three needles are spaced at 1 mm increments vertically; each of the three uppermost needles is at 6 mm radial spacing from the uppermost heater needle.

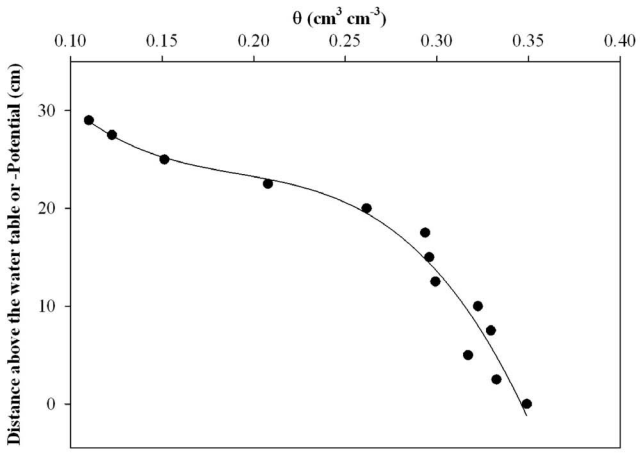

Figure 2. Initial volumetric water content (θ) at different depths in the drained column with water table at 29 cm depth. These data also correspond to water retention for the 0 to −30 cm potential range.

data shown for 0 to −30 cm range). Eleven-needle heat-pulse probes (Figure 1b details in section 2.2) were used for measurement of soil temperature and thermal properties. In addition to heat-pulse data collected during the experiments (described below), the soil thermal conductivity (λ)-volumetric water content (θ) relationship for the sand was determined independently by packing the soil in a separate column at a bulk density = 1.65 g cm^{-3} and measuring λ at various θ using the KD2 Pro Thermal Property Sensor (Decagon Devices Inc., Pullman, WA). The observed λ-θ relationship for this soil closely matches the *Chung and Horton* [1987] model for λ for sandy soils (Figure 3).

2.2. Soil Heat Balance

[9] The SHB approach was proposed by *Heitman et al.* [2008b, 2008c] as a method for estimating subsurface evaporation. Fine-scale temperature and thermal property measurements collected with heat-pulse probes (HPP) are used to compute the heat balance for a soil layer. For this study, heat-pulse measurements were taken using an 11-needle HPP [*Zhang et al.*, 2012]. All 11 needles of the HPP contained 40-gauge type E (chromel-constantan) thermocouples for temperature measurement (Figure 1b). The four longer needles also contained a resistance heater made of 38-gauge Nichrome 80 wire for producing a heat pulse. Further details on the HPP design are given by *Zhang et al.* [2012]. The HPP was installed in vertical orientation with its needles parallel to the soil surface and the top needle barely covered with soil. The HPP was used for two functions: (1) collecting soil temperature data each hour to assess temperature gradients imposed between the surface and subsurface boundaries of the soil column; and (2) making heat-pulse measurements from each heater needle every 2 h to determine soil thermal properties.

[10] Measurements included soil temperatures at all 11 needle locations at 0, 1, 2, 6, 12, 18, 24, 30, 36, 42, and 48 mm depths followed by heat-pulse measurements via two heaters at a time. Heaters 1 and 3, located at 6 and 30 mm depth, respectively, were activated together after one ambient temperature measurement; and heaters 2 and

Table 1. Particle Size Distribution, by Diameter and Weight, of the Soil Used in the Study

Clay	Silt	Very Fine Sand	Fine Sand		Medium Sand		Coarse Sand		Very Coarse Sand
Particle Diameter, mm[a]									
0.002	0.002–0.053	0.053–0.106	0.106–0.180	0.180–0.250	0.250–0.355	0.355–0.500	0.500–0.710	0.710–1.000	1.000–2.000
% Particles by Weight									
0	0	2.1	6.9	11.6	29.7	27.2	14.3	6.1	2.2

[a]Size separate classifications are according to USDA-NRCS system.

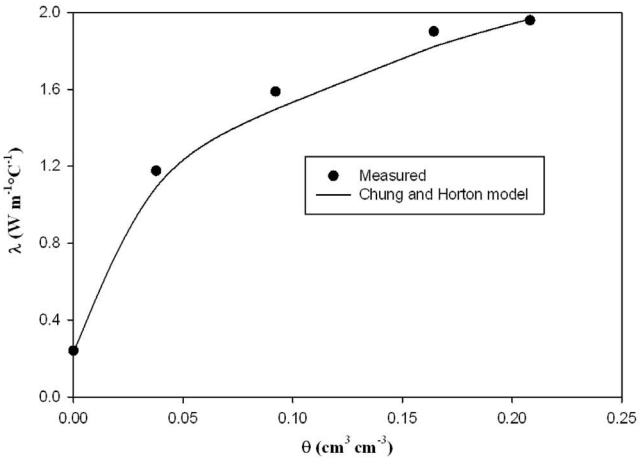

Figure 3. Soil thermal conductivity (λ) as it varies with water content (θ) for the soil used in the experiments. Measurements were collected at bulk density = 1.65 g cm^{-3}. The *Chung and Horton* [1987] model for sandy soil is shown for comparison.

4, located at 18 and 42 mm depths, respectively, were activated together after the next ambient temperature measurement 1 h later. The heaters were activated for 8 s. Temperature traces of the needles adjacent to the heaters were recorded at 0.5 s intervals for a total of 100 s during each heat pulse measurement. A 1 h recovery period was given after each heat-pulse cycle to allow local temperatures to return to ambient temperature before the next soil temperature measurement. A data logger (CR 3000, Campbell Scientific, Logan, UT) was used to collect temperature and heat-pulse data. Temperature responses of needles adjacent to heater needles were used to compute soil thermal diffusivity and volumetric heat capacity following *Bristow et al.* [1994] and *Knight and Kluitenberg* [2004], respectively, and thermal conductivity (λ) was determined as the product of thermal diffusivity and volumetric heat capacity.

[11] Temperature and thermal property data were used as described by *Zhang et al.* [2012] to compute the sensible heat balance for different soil layers with layer boundaries corresponding to the middle of adjacent needles. Latent heat flux originating from these layers was estimated following the sensible heat balance for a soil layer [*Gardner and Hanks*, 1966]:

$$LE = (H_1 - H_2) - \Delta S, \quad (1)$$

where LE is the latent heat flux, H_1 and H_2 are the conduction heat fluxes at upper and lower boundaries of the soil layer, respectively, and ΔS is the change in sensible heat storage for the layer.

[12] Heat flux at the middle location of two adjacent needles was calculated from temperature gradient and heat pulse estimated λ. For calculating the temperature gradient, apparent spacing between the needles was determined by calibrating the probe in agar-stabilized water before probe installation [*Campbell et al.*, 1991]. Change in sensible heat storage ΔS was calculated from volumetric heat capacity and the change in ambient temperature of the soil layer during a given time step [*Ochsner et al.*, 2007]. Detailed conceptual background of this method is given by *Heitman et al.* [2008b, 2008c].

2.3. Steady State Evaporation

[13] For the steady state evaporation experiment, the soil was initially saturated and then drained to reach equilibrium with a constantly maintained water table at 29 cm below the soil surface. The upper boundary conditions were constant radiation maintained via the ceramic heat emitter (150 W), zero wind speed, and constant relative humidity (30%) at constant air temperature (20°C). An open pan evaporation rate of 0.7 mm h^{-1} was observed under these boundary conditions. The lower boundary conditions were constant temperature (20°C) at equilibrium with the simulated water table positioned and maintained 29 cm below the soil surface using the Marriott bottle. The initial condition for water content was a drained profile at equilibrium with the water table (Figure 2). The column was left under the described boundary conditions until the soil column mass became constant and a steady change in mass with time was observed for the Marriott bottle, indicating steady state evaporation conditions. Steady state evaporation was observed (via mass measurements) after approximately 70 h. Thereafter, both SHB and mass balance measurements were recorded from 72 to 120 h.

2.4. Transient Evaporation

[14] For the transient evaporation experiment, the same soil column set up as the steady state evaporation study was used, except that there was no external water supply to the column during the study. The column was first saturated and drained such that the initial water content condition was a drained profile (Figure 2) with a water table at 29 cm depth. Water supply to the column was then disconnected at 0 h. At the same time, the heat emitter was turned on to maintain a constant radiation load at the soil surface. As before, an open pan evaporation of 0.7 mm h^{-1} was observed under the experimental conditions. Mass-loss evaporation, soil temperature, and heat-pulse data were collected for a period of 90 h.

3. Results and Discussion

3.1. Steady State Evaporation

[15] After attaining near steady state evaporation at approximately 70 h, an average mass balance evaporation rate of 0.28 mm h^{-1} (ranging 0.26–0.32 mm h^{-1}) was observed from 72 to 120 h, when the experiment was terminated. This evaporation rate, approximately 40% of pan evaporation (0.7 mm h^{-1}) recorded under the same surface boundary conditions, indicates soil-limited evaporation. After 70 h of drying under these conditions, the soil surface was visibly dry, indicating formation of a DSL and shift in control of evaporation from atmosphere to soil.

[16] Figure 4a shows the temperature profile near the surface of the column. The steepest temperature gradient was observed for the 0–1 mm soil layer. The inflection point in the temperature profile was at approximately 1 mm, suggesting a heat sink and/or a sharp contrast in soil thermal properties [*Heitman et al.*, 2008a]. Calculating heat flux requires a known temperature gradient and λ at the depth of interest. In this study, using the 11-needle HPP, we

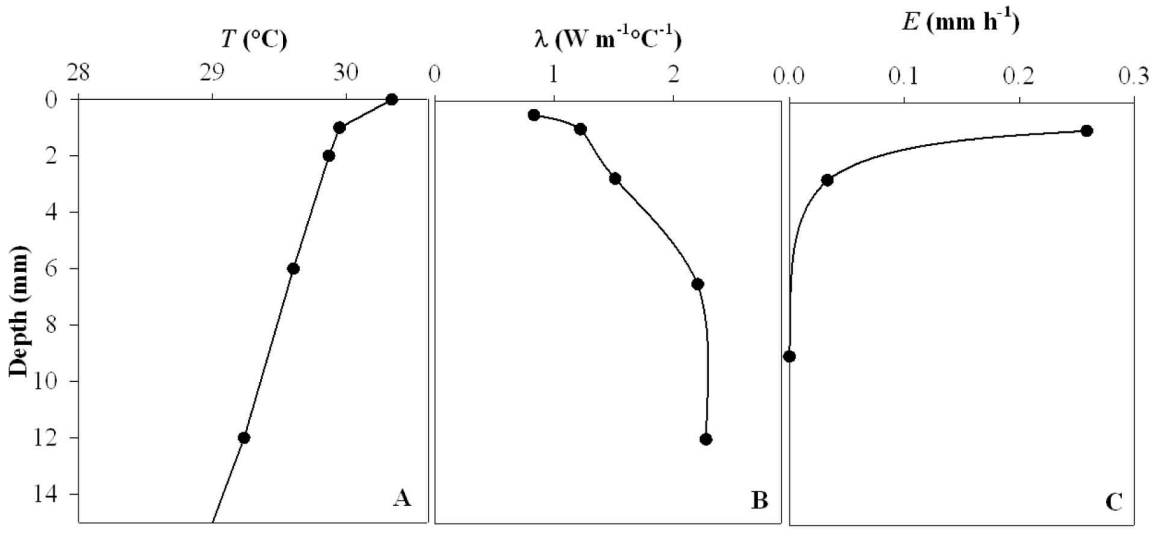

Figure 4. (a) Temperature (T) profile during steady state evaporation. Note that temperature at the lower boundary (34 cm depth, not shown) was maintained at 20 °C for the entire duration of the study. (b) Thermal conductivity (λ) profile during steady state evaporation measured with the heat-pulse method. Values for the 0–1 and 1–2 mm depth increments were estimated as described in the text. (c) Steady state subsurface evaporation (E) from different depth layers determined by the sensible heat balance approach during the constant rate evaporation.

were able to measure near-surface temperature gradients for 0–1, 1–2, and 2–4 mm layers. Thermal properties of the 0–1 and 1–2 mm layers cannot be measured directly using the HPP because the first heater needle is located at 6 mm depth (6 mm radial distance from the needles at 1 and 2 mm depths) in accordance with geometric constraints imposed by the heat-pulse method [*Zhang et al.*, 2012]. We were, however, able to detect differences in thermal properties of the 0–6, 1–6, and 2–6 mm depth layers based on temperature responses at 0, 1, and 2 mm depths to the heat input from the heater needle at 6 mm depth.

[17] Thermal conductivities of 1.35, 1.45, and 1.51 W/(m°C) were recorded for the 0–6, 1–6, and 2–6 mm layers, respectively. A comparison between λ of the 0–6 mm layer and that of the 2–6 mm layer shows that including the surface 0–2 mm depth increment resulted in significant decrease in bulk λ for the 0–6 mm depth layer. Alternately, λ for the 1–6 mm layer is relatively close to that of the 2–6 mm layer. This suggests that the 0–1 mm layer had much lower λ as compared to the wetter subsurface layer. Thermal resistance of a layer per unit area can be expressed as the ratio of thickness of the layer to the thermal conductivity of the layer. For heat flow perpendicular to soil layers, effective thermal resistance will be equal to the sum of thermal resistance values of constituent layers (analogous to resistance in series). Hence, the effective thermal resistance is equal to the depth-weighted harmonic mean of the thermal conductivities of constituent layers. By assuming λ for the 1–6 mm layer as a depth-weighted harmonic mean of λ for the 1–2 and 2–6 mm layers, and treating λ for the 1–2 mm layer as the unknown, we estimated λ of the 1–2 mm layer to be 1.22 W/(m°C). Similarly, by assuming λ for the 0–6 mm layer as a harmonic mean of λ for the 0–1, 1–2, and 2–4 mm layers with λ of the 0–1 mm layer unknown, we estimated λ for the 0–1 mm layer to be 0.83 W/(m°C). Thus, a complete near-surface thermal property profile was obtained (Figure 4b).

[18] Soil samples were collected destructively from the 0–1 and 1–2-mm soil layers of the experimental soil column under steady state evaporation conditions. Water content of the collected samples was determined gravimetrically and converted to θ using the column bulk density. Thermal conductivity corresponding to measured θ of the 0–1 and 1–2 mm depth layers from the independently obtained λ-θ relationship (Figure 3) were 0.75 and 1.05 W/(m°C), respectively. These values were similar to the estimated values of 0.83 and 1.22 W/(m°C), respectively, indicating that the estimated values well represented thermal properties in the "undetectable" near-surface zone described by *Sakai et al.* [2011].

[19] Evaporation rates estimated using the SHB (equation (1)) were 0.26 and 0.03 mm h^{-1} for the 0.5–1.5 and 1.5–4 mm layers, respectively, with no measureable evaporation in deeper layers (Figure 4c). In the full evaporation zone of 0–4 mm, 90% of evaporation occurred in the 0.5–1.5 mm layer, which corresponds with the inflection point in the temperature profile (Figure 4a). This peak rate of evaporation within the 0–2 mm layer indicates that the downward migration of the DSL was restricted by the constant water supply from the relatively shallow water table.

[20] The depth-integrated evaporation rate (i.e., summation of evaporation rate for all depth increments) estimated by the SHB approach was 0.29 mm h^{-1} (ranging 0.25–0.35 mm h^{-1}) for the 0.5–4 mm layer during the 48 h observation period. This was close to the average evaporation rate of 0.28 mm h^{-1} (ranging 0.26–0.32 mm h^{-1}) determined by the mass balance approach, with a difference of only 0.01 mm h^{-1}. These results, which constitute the first test of the SHB

approach under controlled laboratory conditions, support less precise tests under field conditions [*Heitman et al.*, 2008b, 2008c; *Xiao et al.*, 2011], as well as numerical studies for isothermal and nonisothermal conditions [*Sakai et al.*, 2011], and demonstrate that the SHB approach is accurate for measuring the in situ, subsurface evaporation rate.

3.2. Transient Evaporation

[21] As described before, for the transient experiment, the water supply was disconnected and the heat emitter was turned on at time 0. Immediately after turning on the heat emitter, a high mass balance evaporation rate of 0.61 mm h^{-1}, comparable to pan evaporation rate of 0.7 mm h^{-1}, was recorded in the first hour. The mass balance evaporation rate dropped to 0.38 mm h^{-1} by 5 h (Figure 5) and remained nearly constant until approximately 40 h. Experimental conditions essentially resulted in very short-lived stage-1 type conditions (<2 h) followed by a period of near-constant stage-2 evaporation (2 to 40 h), buoyed by water storage in the bottom of the column. The initial condition of a drained profile with water table at 29 cm left 5 cm of saturated soil at the bottom of the column. This provided a water supply for maintaining the evaporation front close to the surface, but the rate at which water was supplied was not enough to maintain evaporation at potential rate. This resulted in a near-constant, soil-limited evaporation from 2 to 40 h and prolonged the period before transient falling-rate evaporation was observed. The soil surface became visibly dry around 30 h into the drying period. A steep decrease in evaporation rate was observed from 40 to 78 h with evaporation rates decreasing from 0.33 to 0.14 mm h^{-1}. A relatively low and constant evaporation rate (approximately 0.14 mm h^{-1}) was observed from 78 to 90 h (when measurements were discontinued), possibly indicating stage-3 evaporation.

[22] Figure 6a shows soil temperature profiles for the 0–18 mm layer at different times during the transient evaporation experiment. The shape of the temperature profile remained almost constant from 1 to 10 h with approximately 3.5°C increase in ambient temperature. About 1°C increase in temperature was observed from 10 to 30 h. A comparison between 30 and 40 h shows that the temperature profile for 0–2 mm depth layer became steeper at 40 h. This change in soil temperature profile at 40 h coincides with the beginning of a steep decrease in mass balance evaporation rates (Figure 5). The temperature profile for the 2–6 mm depth layer is steeper at 50 h as compared to that at 40 h. The temperature profile in the 6–12 mm depth zone became relatively steep at 70 h as compared to that at 50 h. The soil temperature profile remained almost the same from 80 to 90 h. This coincides with the low, constant mass balance evaporation rate during this period (Figure 5).

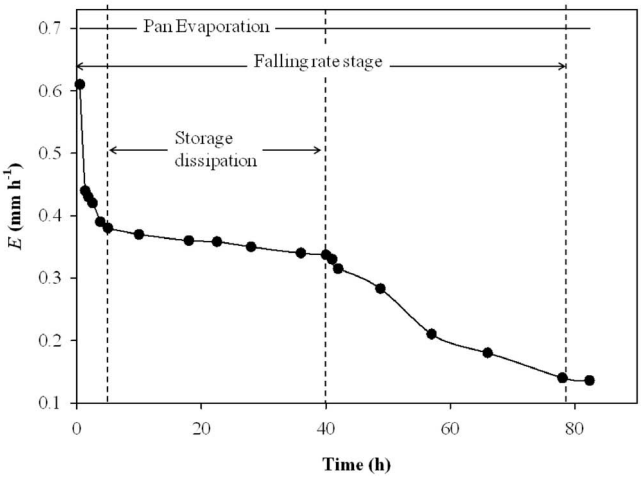

Figure 5. Evaporation (E) from the soil column determined by mass balance during transient evaporation.

[23] For the steady state evaporation experiment (section 3.1), the thermal property profile remained constant with time, which allowed precise λ estimates by repeated heat-pulse measurements under the same conditions. Similar efforts under transient conditions produced inconsistent results. So, for the transient experiment, heat-pulse estimated λ for the 0–6 and 1–6 mm layers were used directly for heat flux calculations at 0.5 and 1.5 mm depths following *Zhang et al.* [2012]. Near-surface λ profiles at different times during transient evaporation experiment are shown in Figure 6b. The data show a decreasing trend in near-surface λ with drying from 10 to 90 h. At 10 h, λ ranged from approximately 0.76 W/(m°C) in the surface 2 mm to 1.4 W/(m°C) for 4 mm and deeper. From 10 to 20 h, λ at 4 mm and deeper decreased by approximately 0.2 W/(m°C), whereas the respective decrease in λ was only 0.08 W/(m°C) for the upper 2 mm depth. A more pronounced decline in λ was observed from 20 to 30 h with about 0.3 W/(m°C) decrease in λ in the 0–12 mm layer. Thereafter, λ continued to decrease, though more subtly, from 30 to 80 h. After 40 h, the λ for 0–2 mm was very low [0.45 W/(m°C)], equivalent to a θ of approximately 0.01 m^3 m^{-3} (Figure 3), indicating an almost air-dry 0–2 mm layer from 40 h onwards. The λ profile remained almost constant from 80 to 90 h corresponding to the period of low and constant mass balance evaporation.

[24] Using temperature and λ profiles shown in Figure 6, total subsurface evaporation rates of 0.21 and 0.28 mm h^{-1} were observed at 28 and 32 h, respectively. These values were lower than the mass balance evaporation rates of 0.35 and 0.34 mm h^{-1} at the same times, respectively. These data indicate that at 28 and 32 h some evaporation was still taking place at the surface or shallower than the 0.5 mm depth. An increasing proportion of evaporation originating from the subsurface with progressive drying (0.21 mm h^{-1} at 28 h and 0.28 mm h^{-1} at 32 h) suggests a transition from surface to subsurface (depth > 0.5 mm) evaporation.

[25] Figure 7 shows SHB estimated subsurface evaporation rates in comparison to mass evaporation at 40 h and thereafter. Total subsurface evaporation rates estimated by the SHB approach were 0.36, 0.23, 0.17, and 0.14 mm h^{-1} at 40, 56, 66, and 78 h, respectively, which were close to the mass evaporation rates of 0.33, 0.21, 0.18, and 0.14 mm h^{-1} observed at the same times, respectively. This period corresponded to the falling rate evaporation stage indicated by a steep fall in mass balance evaporation rates between 40 and 78 h. At 40 h, the SHB estimated evaporation rate (0.36 mm h^{-1}) originated from the 1.5–4 mm depth layer indicating a very narrow evaporation zone close to the surface (Figure 8). With further drying of the soil, the evaporation front moved deeper and widened from 40 to 66 h, eventually reaching a very low evaporation rate

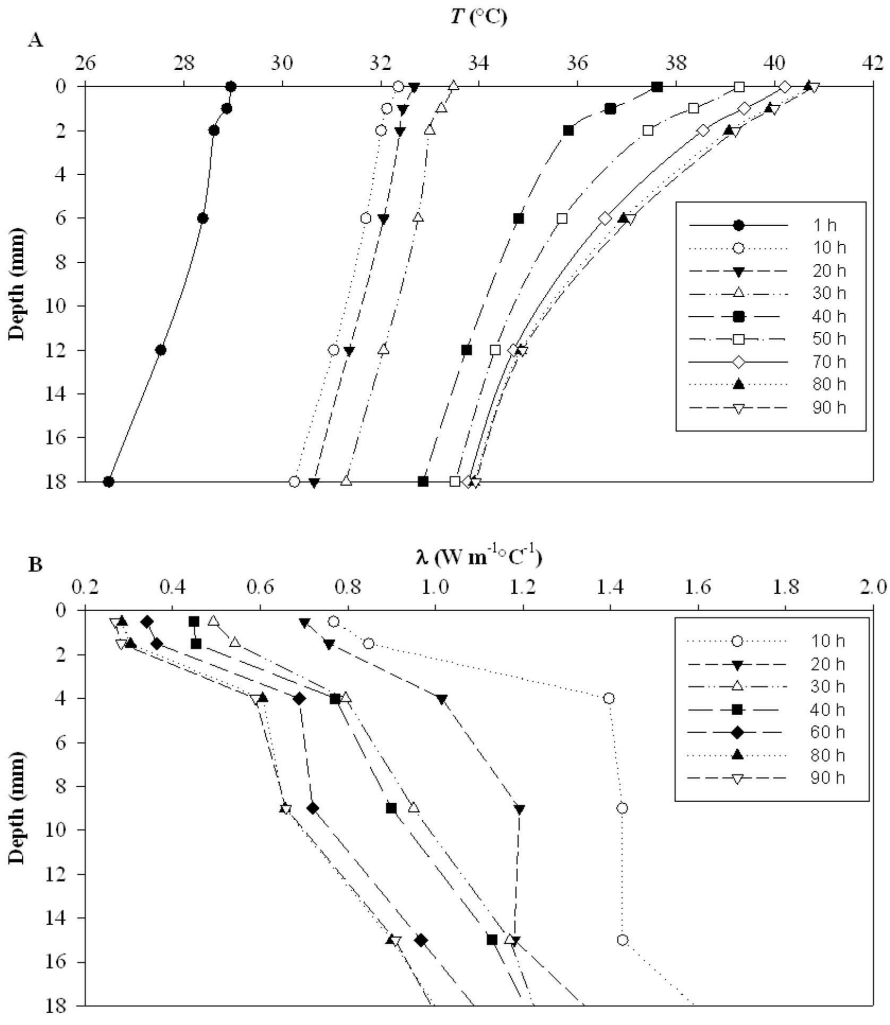

Figure 6. (a) Near-surface soil temperature (T) profiles during transient evaporation. Note that T at the lower boundary (34 cm depth, not shown) was maintained at approximately 20°C for the duration of the study. (b) Measured thermal conductivity (λ) during transient evaporation.

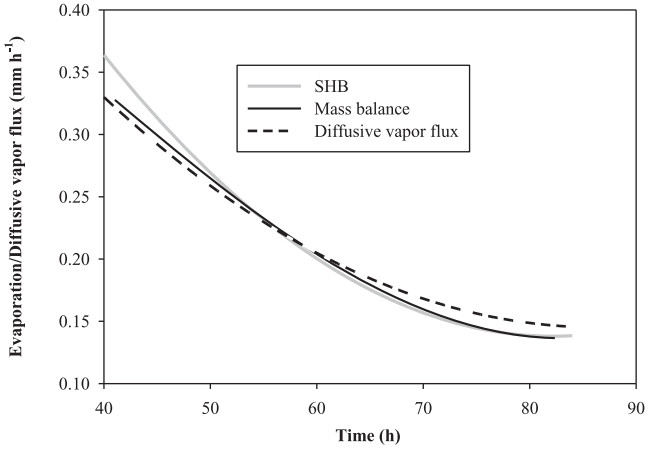

Figure 7. Evaporation rate determined by the sensible heat balance (SHB) and mass balance approaches and diffusive vapor flux during the transient stage-2 evaporation.

of 0.14 mm h^{-1} at 78 h with 77% of evaporation occurring in the 9–15 mm depth layer. Later at 84 h, the subsurface evaporation rate stayed the same as that observed at 78 h (possibly indicating stage-3 evaporation) but the evaporation front narrowed, with all of the subsurface evaporation occurring in the 9–15 mm layer.

[26] Comparison of the SHB estimated evaporation with mass balance data shows that there was a transition from surface to subsurface evaporation, with some evaporation occurring below 0.5 mm depth at 28 and 38 h. After 40 h, the SHB estimated evaporation was close to the mass balance evaporation, indicating that evaporation was taking place entirely within the subsurface (below 0.5 mm depth). This suggests that there was a loss of liquid water connectivity to the surface at about 40 h or possibly earlier. This agrees with suggestions by *Idso et al.* [1974] about the loss in liquid water connectivity to the surface at the beginning of falling rate evaporation (stage 2). After this time period, the SHB approach effectively estimated subsurface

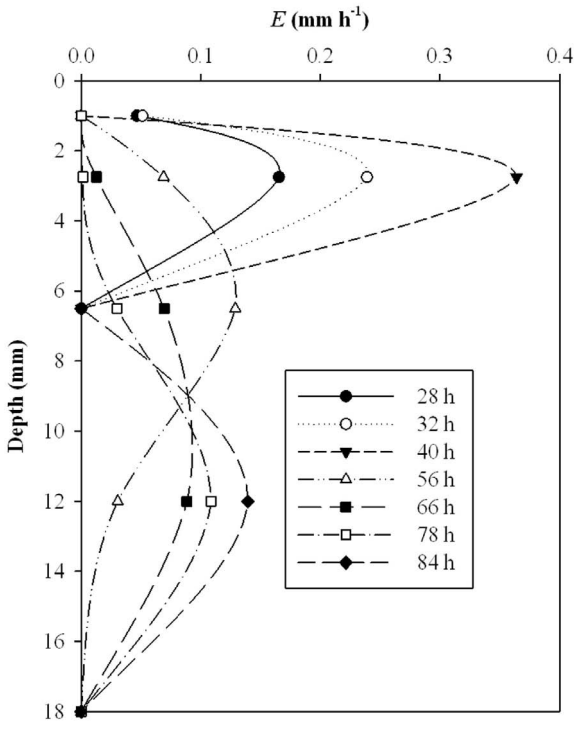

Figure 8. Sensible heat balance estimated subsurface, evaporation (E) profiles at different times during transient evaporation.

evaporation with only 0.01 to 0.03 mm h^{-1} difference between SHB and mass balance. The SHB approach also provided an estimate of the evaporation profile and showed the dynamics of the evaporation front at millimeter scale over a drying event, which has not been demonstrated before, except with numerical modeling [e.g., *Novak*, 2010].

3.3. Estimation of the Thickness of the Dry Surface Layer

[27] The undetectable zone close to soil surface remains a challenge in studying energy and mass transfer with the SHB approach in the highly dynamic near-surface zone [*Sakai et al.*, 2011]. It may not be possible to directly measure thermal properties of this undetectable near-surface zone with sensor designs implemented to date. In the present experiment we were able to detect the differences in λ of the 0–6, 1–6, and 2–6 mm depth zones using an 11-needle HPP. For steady state evaporation conditions, λ profiles remained constant with time, so we were able to further make repeated heat-pulse measurements for estimating λ of different layers. We were also able to test these estimates via destructive sampling. Under transient conditions, however, a similar exercise is cumbersome and probably not feasible.

[28] To further evaluate the implications of heat-pulse estimated thermal properties under transient conditions, we consider an approximate structure for the DSL and underlying soil. After formation of a DSL, the near-surface soil layer is approximately composed of two different zones of contrasting water content and thermal properties (Figure 9). We refer to this near-surface layer as a transition layer where the distributions of moisture and thermal properties are varying rapidly with drying, i.e., the thickness of the DSL changes rapidly under transient conditions. Estimated thickness of the DSL at a given time during a drying period can give important information about the dynamics of the subsurface evaporation front and possible mechanisms for heat transfer.

[29] The near-surface soil layer (transition layer with thickness z_{trans}) can be divided into two zones, a DSL of thickness z_{dry} and a wet subsurface layer of thickness z_{wet}, so that $z_{trans} - z_{wet} = z_{dry}$ (Figure 9). Thermal conductivity

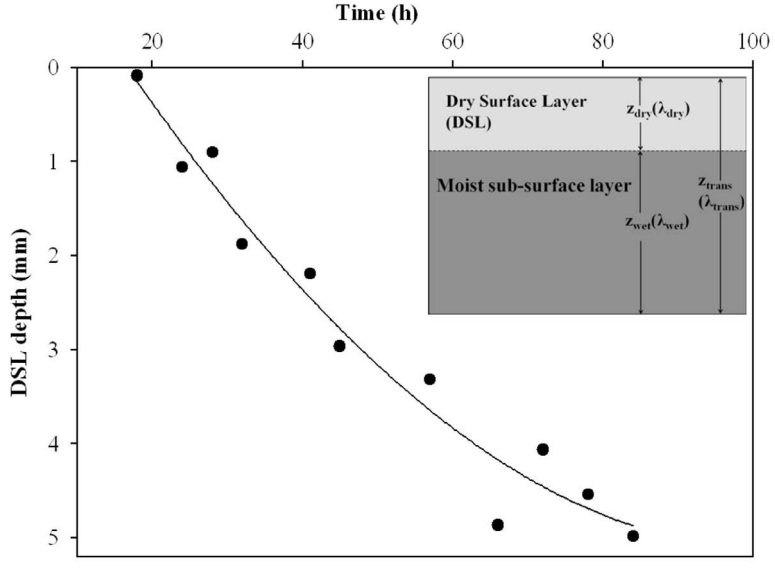

Figure 9. Estimated thickness of the dry surface layer (DSL) during transient evaporation. The line indicates the approximate trend. Inset: Conceptual structure of near-surface transition layer used for estimating thickness of the dry surface layer (DSL) with thickness (z) and thermal conductivity (λ).

of the near-surface transition layer (λ_{trans}) can be expressed as the depth weighted harmonic mean of λ of the constituent layers (as described in section 3.1):

$$\frac{z_{trans}}{\lambda_{trans}} = \frac{z_{dry}}{\lambda_{dry}} + \frac{z_{wet}}{\lambda_{wet}}, \quad (2)$$

where subscripts dry and wet indicate properties for dry and wet layers, respectively.

[30] We estimated λ_{trans} from the bulk heat-pulse measurements in the near-surface layer, i.e., 0–6 mm depth. Thermal conductivity for the wet subsurface layer was estimated from heat-pulse measurements at the bottom boundary of the transition layer, i.e., 6–12 mm depth. Thermal conductivity of the DSL (λ_{dry}) was estimated from independent measurements of dry soil at the same bulk density. The thickness of the DSL (z_{dry}) could then be calculated from equation (2) and heat-pulse measurements collected throughout the evaporation experiments. *Kluitenberg et al.* [2010] suggested that λ measured by heat-pulse sensors may be more robust than heat capacity and thermal diffusivity measurements (i.e., less sensitive to needle spacing change). Thus we used measured λ for estimation of DSL thickness instead of considering other thermal properties. The estimation of thickness of DSL by equation (2) is independent of evaporation profiles determined from the SHB (described in previous sections) but both are related by using the same heat-pulse determined thermal properties in calculations.

[31] The thickness of the DSL calculated for the steady state evaporation experiment was about 1 mm, which indicates that the evaporation front remained close to the soil surface. The subsurface evaporation estimated by the SHB approach also indicates that about 90% of total evaporation occurred in the 0.5–1.5 mm depth layer. Figure 9 shows the estimated z_{dry} during transient evaporation measurements. The estimated z_{dry} at 18 h was close to zero indicating water connectivity to the soil surface. Estimated z_{dry} reached 1 mm at 28 h and about 2 mm at 40 h. This agrees with the subsurface evaporation of 0.36 mm h^{-1} occurring in the 1.5–4 mm layer as estimated by the SHB approach at 40 h (Figure 8). With progressive drying the evaporation front moved deeper and the estimated z_{dry} increased to 3.3 mm at 56 h, and eventually reached 5 mm at 84 h.

[32] Sensible heat balance evaporation profiles show that evaporation was mainly occurring below the estimated depth of the DSL for our experimental conditions. This agrees with previous studies indicating that vaporization of water occurs at the bottom boundary of the DSL [*Hillel*, 1971; *Campbell*, 1985; *Yamanaka et al.* 1998] and liquid water connectivity to the surface is lost at the beginning of falling rate/stage-2 evaporation [*Idso et al.*, 1974].

3.4. Diffusive Vapor Flux During Transient Stage-2 Evaporation

[33] We estimated diffusive water vapor flux for stage-2 evaporation from 40 h onwards in the transient experiment, i.e., for the period when SHB subsurface evaporation profiles indicated that all the evaporation was occurring in the subsurface (Figure 8). The diffusive vapor flux (J) was calculated according to Fick's Law (equation (3)) using DSL thickness estimated in section 3.3 and the diffusion coefficient model for dry porous media given by *Millington* [1959]:

$$J = \varepsilon^{4/3} D \frac{e_{soil} - e_{air}}{z_{dry}}, \quad (3)$$

where ε is the soil air-filled porosity, D is the diffusion coefficient of vapor in free air (2.57×10^{-5} m^2 s^{-1}), $e_{soil} = 3.03 \times 10^{-2}$ kg m^{-3} is water vapor density at the drying front, and $e_{air} = 5.2 \times 10^{-3}$ kg m^{-3} is water vapor density in the air above the column at ambient air temperature (20°C) and humidity (30%).

[34] Figure 7 shows that calculated J closely matches evaporation determined by the SHB and mass balance approaches during transient stage-2 evaporation. This further supports results from the SHB indicating that liquid water connection to the surface is lost early in the falling rate stage of evaporation (stage 2). Studies under isothermal conditions also showed "jumps" in the evaporation plane from the surface to the subsurface at the end of stage 1, but liquid water connectivity to the surface was reported to be lost at the onset of low, constant rate evaporation [*Shokri and Or*, 2011]. These jumps were reported to be affected primarily by porous media properties. However, under nonisothermal conditions, we observed steep temperature gradients in the near surface as compared to the underlying subsurface layers, in agreement with previous studies [*Heitman et al.*, 2010, *Xiao et al.*, 2011, *Zhang et al.*, 2012]. This sharp temperature gradient suggests the importance of energy transfer driven by the radiation boundary condition, which may drive the formation and downward migration of the DSL for nonisothermal conditions.

[35] Together, our observations suggest that under nonisothermal conditions, the DSL forms early in the falling rate stage of evaporation. Evaporation then occurs in the subsurface. The zone of subsurface evaporation is narrow and close to the surface at the beginning (Figure 8). With progressive drying, the thickness of the DSL increases (Figure 9) and the evaporation front moves deeper and widens, eventually becoming narrow again at the end of the falling rate stage (Figure 8). It is evident that under nonisothermal conditions, temperature gradients in addition to hydraulic properties of porous media play an important role in evaporation dynamics, resulting in relatively quick drying of the soil surface and formation of a DSL early in falling rate evaporation. After formation of a DSL, evaporation occurs in the subsurface and evaporated water is transferred to the atmosphere via vapor diffusion through the DSL. These results are consistent with a number of previous reports [e.g., *Hillel*, 1971; *Idso et al.*, 1974; *Hillel*, 1980; *Campbell*, 1985, *de Vries and Philip*, 1986; *Mayocchi and Bristow*, 1995; *Yamanaka et al.*, 1997; *Yamanaka et al.*, 1998; *Heitman et al.*, 2008b, 2008c; *Shokri et al.*, 2009, *Heitman et al.*, 2010; *Novak*, 2010], but differ from recent studies suggesting loss of hydraulic connection to the surface at the onset of stage 3 for isothermal conditions [e.g., *Shokri and Or*, 2011].

4. Summary and Conclusions

[36] Nonisothermal evaporation is a complex process involving both mass and energy transfer. To date, understanding of the transition between atmospherically controlled

and late stage evaporation remains limited. The results from our study show that the SHB approach effectively estimated the subsurface evaporation rate with only 0.01–0.03 mm h^{-1} difference from the mass balance evaporation rate under steady state as well as transient stage-2 evaporation conditions. The SHB approach also provided measurement-based quantification of subsurface, nonisothermal evaporation profiles (i.e., the distribution of the evaporation zone) at millimeter scale under transient conditions over a drying event. Subsurface evaporation matched mass balance in the early falling rate stage, indicating a loss in liquid water connectivity to the surface. Further studies under a wider range of textures and under natural radiation conditions can improve our knowledge of soil water evaporation, especially at the onset and during falling rate evaporation when the evaporation front shifts from the surface to the subsurface.

[37] It remains challenging to directly measure thermal properties of the "undetectable" zone near the soil surface. However, the observed ability of HPPs to detect differences in thermal properties of 0–6, 1–6, and 2–6 mm depth zones in the present experiments opens the possibility of a measurement-based estimate of thermal property profiles for the highly dynamic near-surface zone. We used heat-pulse measurements along with independent measurements of λ for dry soil to continuously estimate the thickness of the DSL over a drying period. The estimated thickness of the DSL was used to compute diffusive vapor flux with Fick's law, which closely matched the mass balance evaporation and subsurface evaporation estimated by the SHB approach.

[38] Measurement-based estimates of near-surface thermal property profiles, DSL thickness, and the capability of the SHB approach to estimate millimeter-scale evaporation profiles provides an opportunity to test existing theories and can help in developing new models capable of precise estimates of near-surface energy and mass transfer occurring at the land surface. The improved knowledge about the soil water evaporation process and near-surface energy and mass transfer will influence research and understanding of various natural processes occurring at wide range of scales (e.g., microclimate for seeds and microbes in the near-surface to large scale hydrologic and climatic patterns), and has a wide range of applications, such as agricultural and forestry water management and conservation, evaporation from landfill covers, industrial drying processes, and vapor fluxes of various substances from the land surface.

[39] **Acknowledgments.** This work was supported by the National Science Foundation under grants 0809656 and 1215864 and US-Israel Bination Agricultural Research and Development Fund.

References

Arya, L. M., D. C. Bowman, B. B. Thapa, and D. K. Cassel (2008), Scaling soil water characteristics of golf course and athletic field sands from particle size distribution, *Soil Sci. Soc. Am. J.*, *72*, 25–32, doi:10.2136/sssaj2006.0232.

Arya, L. M., J. L. Heitman, B. B. Thapa, and D. C. Bowman (2010), Predicting saturated hydraulic conductivity of golf course sands from particle-size distribution, *Soil Sci. Soc. Am. J.*, *74*, 33–37, doi:10.2136/sssaj2009.0022.

Bittelli, M., F. Ventura, G. S. Campbell, R. L. Snyder, F. Gallegati, and P. R. Pisa (2008), Coupling of heat, water vapor, and liquid water fluxes to compute evaporation in bare soils, *J. Hydrol.*, *362*, 191–205, doi:10.1016/j.jhydrol.2008.08.014.

Bristow, K. L., G. J. Kluitenberg, and R. Horton (1994), Measurement of soil thermal properties with a dual-probe heat-pulse technique, *Soil Sci. Soc. Am. J.*, *58*, 1288–1294.

Brutsaert, W., and D. Chen (1995), Desorption and the two stages of drying of natural tallgrass praire, *Water Resour. Res.*, *31*, 1305–1313.

Campbell, G. S. (1985), *Soil Physics With Basic Transport Models for Soil-Plant System*, Elsevier, New York.

Campbell, G. S., C. Calissendorff, and J. H. Williams (1991), Probe for measuring soil specific heat 2 using a heat-pulse method, *Soil Sci. Soc. Am. J.*, *55*, 291–293.

Chung, S. O., and R. Horton (1987), Soil heat and water flow with a partial surface mulch, *Water Resour. Res.*, *23*, 2175–2186.

de Vries, D. A., and J. R. Philip (1986), Soil heat flux, thermal conductivity, and the null-alignment method, *Soil Sci. Soc. Am. J.*, *50*, 12–18.

Feddes, R. A. (1971), Water, heat and crop growth, Ph.D. thesis, 184 pp. Comm. Agric. Univ., Institute of Land and Water Management Research, Wageningen.

Gardner, H. R., and R. J. Hanks (1966), Evaluation of the evaporation zone in soil by measurement of heat flux, *Soil Sci. Soc. Am. J.*, *30*, 425–428.

Heitman, J., R. Horton, T. Ren, I. Nassar, and D. Davis (2008a), A test of coupled soil heat and water transfer prediction under transient boundary temperatures, *Soil Sci. Soc. Am. J.*, *72*, 1197–1207.

Heitman, J. L., R. Horton, T. J. Sauer, and T. M. DeSutter (2008b), Sensible heat observations reveal soil-water evaporation dynamics, *J. Hydromet.*, *9*, 165–171.

Heitman, J. L., X. Xiao, R. Horton, and T. J. Sauer (2008c), Sensible heat measurements indicating depth and magnitude of subsurface soil water evaporation, *Water Resour. Res.*, *44*, W00D05, doi:10.1029/2008WR006961.

Heitman, J. L., R. Horton, T. J. Sauer, T. S. Ren, and X. Xiao (2010), Latent heat in soil heat flux measurements, *Agric. For. Meteor*, *150*, 1147–1153.

Hillel, D. (1971), *Soil and Water: Physical Principles and Processes*, Academic, New York.

Hillel, D. (1980), *Applications of Soil Physics*, Academic Press, New York, 385 pp.

Howard, A., J. L. Heitman, and D. Bowman (2010), A simple approach for demonstrating water retention and field capacity, *J. Nat. Res. Life Sci. Ed.*, *39*, 120–124.

Idso, S. B., R. J. Reginato, R. D. Jackson, B. A. Kimball, and F. S. Nakayama (1974), The three stages of drying of a field soil, *Soil Sci. Soc. Am. Proc.*, *38*, 831–837.

Idso, S. B., R. D. Jackson, and R. J. Reginato (1975), Estimating evaporation: A technique adaptable to remote sensing, *Science*, *189*, 991–992.

Jalota, S. K., and S. S. Prihar (1998), *Reducing Soil-Water Evaporation With Tillage and Straw Mulching*, p. 142, Iowa State University Press, Ames, IA.

Kimball, B. A. (1973), Water vapor movement through mulches under field conditions, *Soil Sci. Soc. Am. Proc.*, *37*, 813–818.

Kluitenberg, G. J., T. Kamai, and J. A. Vrugt (2010), Effect of probe deflection on dual-probe heat-pulse thermal conductivity measurements, *Soil Sci. Soc. Am. J.*, *74*(5), 1537–1540.

Knight, J. H., and G. J. Kluitenberg (2004), Simplified computational approach for the dual-probe heat-pulse method, *Soil Sci. Soc. Am. J.*, *68*, 447–449.

Lemon, E. R. (1956), The potentialities for decreasing soil moisture evaporation loss, *Soil Sci. Soc. Am. Proc.*, *20*, 120–125.

Liu, B. C., W. Liu, and S. W. Peng (2005), Study of heat and moisture transfer in soil with a dry surface layer, *Int. J. Heat Mass Transfer*, *48*(21–22), 4579–4589.

Mayocchi, C. L., and K. L. Bristow (1995), Soil surface heat flux: Some general questions and comments on measurements, *Agric. For. Meteor. 75*, 43–50.

Millington, R. J. (1959), Gas diffusion in porous media,. *Science*, *130*, 100–102.

Novak, M. D. (2010), Dynamics of the near-surface evaporation zone and corresponding effects on the surface energy balance of a drying bare soil, *Agric. For. Meteor.*, *150*, 1358–1365.

Ochsner, T. E., T. J. Sauer, and R. Horton (2007), Soil heat storage measurements in energy balance studies, *Agron. J.*, *99*, 311–319.

Sakai, M., S. B. Jones, and M. Tuller (2011), Numerical evaluation of subsurface soil water evaporation derived from sensible heat balance, *Water Resour. Res.*, *47*, W02547, doi:10.1029/2010WR009866.

Shokri, N., and D. Or (2011), What determines drying rates at the onset of diffusion controlled stage-2 evaporation from porous media? *Water Resour. Res.*, *47*, W09513, doi:10.1029/2010WR010284.

Shokri, N., and G. D. Salvucci (2011), Evaporation from porous media in the presence of a water table, *Vadose Zone J.*, *10*, 1–10.

Shokri, N., P. Lehmann, and D. Or (2009), Critical evaluation of enhancement factors for vapor transport through unsaturated porous media, *Water Resour. Res.*, *45*, W10433, doi:10.1029/2009WR007769.

Snyder, R. L., K. Bali, F. Ventura, and H. Gomez-Macpherson (2000), Estimating evaporation from bare or nearly bare soil., *J. Irrig. Drain. Eng.*, *126*(6), 399–403.

Ventura, F., B. Faber, K. Bali, R. L. Snyder, D. Spano, P. Duce, and K. F. Schulbach (2001), A model for estimating evaporation and transpiration from row crops, *J. Irrig. Drain. Eng.*, *127*(6), 339–345.

Xiao, X., R. Horton, T. Sauer, J. L. Heitman, and T. Ren (2011), Cumulative soil water evaporation as a function of depth and time, *Vadose Zone J.*, *10*, 1016–1022.

Yamanaka, T., and J. Shimada (1997), Simple but reliable method to extract soil water for stable isotope analysis, *J. Jpn. Soc. Hydrol. Water Resour.*, *10*, 181–184, in Japanese with English abstract.

Yamanaka, T., and T. Yonetani (1999), Dynamics of the evaporation zone in dry sandy soils, *J. of Hydrol.*, *217*(1–2), 135–148.

Yamanaka, T., A. Takeda, and J. Shimada (1998), Evaporation beneath the soil surface: Some observational evidence and numerical experiments, *Hydrol. Processes*, *12*, 2193–2203.

Zhang, X., J. L. Heitman, R. Horton, and T. Ren (2012), Measuring subsurface soil-water evaporation with an improved heat-pulse probe. *Soil Sci. Soc. Am. J.*, *76*, 876–879.